

# Correlation between the curvature and various properties of the neutron star

S. K. Biswal<sup>1</sup> , H. C. Das<sup>2,3</sup> , Ankit Kumar<sup>2,3</sup>, Bharat Kumar<sup>4</sup>, S. K. Patra<sup>2,3</sup>

<sup>1</sup> Department of Astronomy, Xiamen University, Xiamen 361005, P. R. China

<sup>2</sup> Institute of Physics, Sachivalya Marg, Bhubaneswar-751005, India

<sup>3</sup> Homi Bhabha National Institute, Training School Complex, Anushakti Nagar, Mumbai 400085, India

<sup>4</sup> Department of Physics & Astronomy, National Institute of Technology, Rourkela, India

22 December 2024

## ABSTRACT

We use 30 well-known parameter sets of the relativistic mean-field model to calculate various properties of the neutron star (NS) like mass, radius, central densities and curvature. Predictive competence of the various RMF parameter sets are discussed and compared with observational data of the NICER and GW170817. We try to correlate some properties of the NS like compactness, curvature and radius. We substantiate a correlation between the curvature and compactness of different masses of the NS. The compactness and the curvature of a NS of certain mass shows a strong correlation (0.995 correlation coefficient) for assumed parameter sets. Similarly, we establish another correlation between the radius and curvature of the NS. We also incorporate a three-dimensional correlation between these properties of the NS.

**Key words:** equation of state– stars: neutron– curvature

## 1 INTRODUCTION

Understanding the nature of the fundamental interaction at supra-saturation density is currently considered as a prominent topic in fundamental physics. In the laboratory, we can create the dense matter up to few times of the saturation density (Danielewicz & Lee 2014; Steiner et al. 2010), which is not enough to understand the nuclear interaction at high degree of density and isospin asymmetry. This experimental inadequacy forces us to use neutron star (NS) as sole ingredient to study the high dense nature of the nuclear interaction (Lattimer 2004). NS is one of the most familiar members of the compact object family of the visible universe, having central density 5–6 times the density of the matter at nuclear centre (Baym & Pethick 1979; Lattimer 2004). Most of the terrestrial experiments and analysis of the finite nuclear data give information about the nature of the equation of state (EOS) around saturation density, while the higher density region still remains unexplored. Various theoretical models predict diverge behaviour for the EOSs in that region and that leads to completely different values for the global properties of the NS. The global properties of the NS like maximum mass, radius, moment of inertia be used as an effective tool to put the strong constraints on the nature of the EOS (Lattimer 2004).

Now in the recent years, the tidal deformability from the first binary NS merger event, GW170817 (Abbott et al. 2018, 2017) can also put a spotlight on the nature of matter enclosed inside the NS.

The composition of the NS is not clear till now. In the conventional models, the NS is populated by the neutron and admixture of the proton and electron are inside the NS to maintain the  $\beta$ -equilibrium and charge neutrality conditions. The extreme conditions inside the NS favor various exotic phenomena to happen like hyperon production (Ambartsumyan & Saakyan 1960; Glendenning 1985; Glendenning & Moszkowski 1991), kaon condensation (Glendenning 1985; Glendenning & Schaffner-Bielich 1998, 1999; Christiansen et al. 2000; Gupta & Arumugam 2012, 2013), deconfinement of quark (Collins & Perry 1975; Xia et al. 2016a,b; Xia & Zhou 2017; Dexheimer et al. 2018), and presence of DM particle (Panotopoulos & Lopes 2017; Das et al. 2019; Li et al. 2012; Das et al. 2020c; Ellis et al. 2018; Bhat & Paul 2020; Ciarcelluti & Sandin 2011; Leung et al. 2011). Recently, the NICER (Neutron Star Interior Composition Explorer) data (Raaijmakers et al. 2019; Miller et al. 2019; Bogdanov et al. 2019; Bilous et al. 2019; Riley et al. 2019; Guillot et al. 2019) can put a strong constraints on the mass and radius of a NS. This simultaneous measurement of the mass and radius of a NS can constraint the nuclear EOS. The correlation between the tidal deformability and the radius of the canonical star is now a settled issue (Malik et al. 2018; Hebeler et al. 2010; Lim & Holt 2018; Most et al. 2018; Fattoyev et al. 2018; Tews et al. 2018; Annala et al. 2018; Zhang et al. 2018; Dietrich et al. 2020; Steiner et al. 2010; Capano et al. 2019). But the value of the correlation coefficient is still a debatable issue, various theoretical formalism give different ranges of the correlation coefficients. Similarly, it is noticed that a correlation exists between the skin thickness of the heavy neutron-rich nuclei ( $^{208}\text{Pb}$ ) and NS properties (Fattoyev & Piekarewicz

\* E-mail: subratphy@gmail.com

† harishdas.physics@gmail.com

2012; Horowitz & Piekarewicz 2001). It is the consequence of the fact that the slope of the symmetry energy determine the pressure of the neutron-rich skin and radius of the NS. Li *et al.* have showed that an unique relation between  $K_{sym}$  and slope  $L$  can constrain the high density behaviour of the  $E_{sym}$  (Li & Magno 2020). Along the same path Alam *et al.* have shown that there exist a strong correlation between the NS radii and slope of the incompressibility of the nuclear matter (NM) (Alam *et al.* 2016). Using Brueckner-Hartree-Fock formalism, Wei *et al.* found a strong correlation between NS radius, tidal deformability and pressure of the beta stable matter (Wei *et al.* 2020). Therefore, now it's a common practice to look for a correlation between the NM and NS properties. In this piece of work, we try to find the new type of correlation between properties of the NS. Here, we try to correlate the curvature of NS with other bulk properties like radius and compactness.

According to the general theory of relativity, massive objects warp the space-time which is technically defined or called as curvature. The amount of wraps/strength of curvature depends on the mass of the object. To illustrate this, some mathematical quantities are defined for example the compactness. For a body of Mass  $M$  and radius  $R$ , the compactness is defined as  $\eta = M/R$ . That means massive objects has higher compactness as compared to the lighter one. Like compactness, another quantity is the Riemann tensor, which carries all the information about the space-time curvatures both outside and inside the star. In the previous analysis by Kazim *et al.* (Ekşi *et al.* 2014), they have derived some quantities which are mainly suitable for the measurement of the curvatures of a star. The quantities are  $\mathcal{K}$ ,  $\mathcal{J}$ ,  $\mathcal{R}$  and  $\mathcal{W}$ . Among these four quantities, the quantities  $\mathcal{K}$  and  $\mathcal{W}$  are more prominent to measure the space-time curvature both inside and outside the star. This is because all the components will vanish except ( $\mathcal{R}^1_{010}$ ), even in the outside of the star (Ekşi *et al.* 2014; He *et al.* 2015). Therefore the Kretschmann scalar (square root of full contraction of Riemann tensor) and the square root of full contraction of Weyl tensor are the most significant quantity to measure the curvature of a star. One can find the detailed description for this in Ref. (Ekşi *et al.* 2014) and also a brief formalism is given in sub-section 2.3. In our previous analysis, we have calculated all these defined curvatures with and without dark matter (DM) inside the NS. We found that DM has very significant effects on the curvatures and compactness of the NS. Hence, in this present work, we want to explore more on this curvature and correlate with some other properties of the NS, because the correlations between curvatures and different properties of the NS gives a wider picture about their nature.

This paper is organised as follow, in Sec. 2, we discuss the theoretical formalism of the relativistic mean-field formalism used to calculate the bulk properties of the NS. The last subsection of the Sec. 2 is dedicated to discuss the theoretical formalism various curvature of the NS. In Sec.3, we discuss our result. Finally, Sec. 4 is dedicated to a concluding remark of our results and discussion.

## 2 FORMALISM

In present work, we use relativistic mean-field (RMF) model (Miller & Green 1972; Millener *et al.* 1988; Chin & Walecka 1974; Boguta & Bodmer 1977; Brockmann & Weise 1977; Serot & Walecka 1979; Reinhard 1988; Reinhard *et al.* 1986; Reinhard 1989; Gambhir *et al.* 1990; Ring 1996; Long *et al.* 2004; Meng *et al.* 2006; Nikšić *et al.* 2011; Meng & Zhou 2015) to calculate the EOS of the NS. Since the last few decades, RMF model has been providing a platform to predict the properties of finite and infinite NM. Unlike to the

non-relativistic model, the RMF model obeys the casual limit up to very high-density (Dutra *et al.* 2014). The casual nature of the RMF model provides a natural way to go from finite nuclei to NS, which has a very high density. We use 30 parameter sets of the RMF model to calculate EOS of the NS. These EOS are used to calculate the mass, radius and curvature of the NS.

### 2.1 Mathematical formulation of the RMF model

The RMF model is an effective phenomenological model, where the nucleon-nucleon interaction is modeled through the exchange of effective mesons like  $\sigma$ ,  $\omega$ ,  $\rho$  and  $\delta$ -meson. Non-linear terms of the  $\sigma$  and  $\omega$ -meson are included. The non-linear terms of the  $\sigma$ -meson ( $\sigma^3$  and  $\sigma^4$ ) help to reduce the very high incompressibility of the linear model (Lalazissis *et al.* 2009, 1997) and give an effective three-body interaction effect in RMF model (Reinhard *et al.* 1986; Boguta & Bodmer 1977; Ring 1996; Reinhard 1989). The non-linear  $\omega$ -meson interaction has a significant effects on the EOS at density higher than saturation density. It softens the EOS at a higher density (Sugahara & Toki 1994; Müller & Serot 1996). We start the RMF model with a effective Lagrangian including the various higher order terms of the  $\sigma$ ,  $\omega$ , and  $\rho$ -meson. We write the Lagrangian as follow (Miller & Green 1972; Serot & Walecka 1986; Furnstahl *et al.* 1987; Reinhard 1988; Furnstahl *et al.* 1997; Kumar *et al.* 2017b, 2018):

$$\begin{aligned} \mathcal{L}_{nucl.} = & \sum_{\alpha=\rho,n} \bar{\psi}_\alpha \left\{ \gamma_\mu \left( i\partial^\mu - g_\omega \omega^\mu - \frac{1}{2} g_\rho \vec{\tau}_\alpha \cdot \vec{\rho}^\mu \right) - \left( M_{nucl.} \right. \right. \\ & \left. \left. - g_\sigma \sigma - g_\delta \vec{\tau}_\alpha \cdot \vec{\delta} \right) \right\} \psi_\alpha + \frac{1}{2} \partial^\mu \sigma \partial_\mu \sigma - \frac{1}{2} m_\sigma^2 \sigma^2 \\ & + \frac{\zeta_0}{4!} g_\omega^2 (\omega^\mu \omega_\mu)^2 - \frac{\kappa_3}{3!} \frac{g_\sigma m_\sigma^2 \sigma^3}{M_{nucl.}} - \frac{\kappa_4}{4!} \frac{g_\sigma^2 m_\sigma^2 \sigma^4}{M_{nucl.}^2} \\ & + \frac{1}{2} m_\omega^2 \omega^\mu \omega_\mu - \frac{1}{4} W^{\mu\nu} W_{\mu\nu} + \frac{\eta_1}{2} \frac{g_\sigma \sigma}{M_{nucl.}} m_\omega^2 \omega^\mu \omega_\mu \\ & + \frac{\eta_2}{4} \frac{g_\sigma^2 \sigma^2}{M_{nucl.}^2} m_\omega^2 \omega^\mu \omega_\mu + \frac{\eta_\rho}{2} \frac{m_\rho^2}{M_{nucl.}} g_\sigma \sigma \left( \vec{\rho}^\mu \cdot \vec{\rho}_\mu \right) \\ & + \frac{1}{2} m_\rho^2 \left( \vec{\rho}^\mu \cdot \vec{\rho}_\mu \right) - \frac{1}{4} \vec{R}^{\mu\nu} \cdot \vec{R}_{\mu\nu} - \Lambda_\omega g_\omega^2 g_\rho^2 (\omega^\mu \omega_\mu) \\ & \left( \vec{\rho}^\mu \cdot \vec{\rho}_\mu \right) + \frac{1}{2} \partial^\mu \vec{\delta} \partial_\mu \vec{\delta} - \frac{1}{2} m_\delta^2 \vec{\delta}^2, \end{aligned} \quad (1)$$

where  $M_{nucl.} = 939$  MeV is the mass of the nucleon.  $m_\sigma$ ,  $m_\omega$ ,  $m_\rho$  and  $m_\delta$  are the masses and  $g_\sigma$ ,  $g_\omega$ ,  $g_\rho$  and  $g_\delta$  are the coupling constants for the  $\sigma$ ,  $\omega$ ,  $\rho$  and  $\delta$  mesons respectively. The self interactions of the  $\sigma$ -meson are represented as  $\kappa_3$  and  $\kappa_4$ . Similarly, the  $\zeta_0$  is the self-interacting coupling constants of the  $\omega$  mesons.  $\eta_1$  and  $\eta_2$  are the coupling constants of the  $\sigma$  and  $\omega$ -mesons.  $\Lambda_\omega$  is the crossed coupling constants of the  $\rho$  and  $\omega$ -mesons. The quantities  $W^{\mu\nu}$  and  $\vec{R}^{\mu\nu}$  are the field strength tensors for the  $\omega$  and  $\rho$  mesons respectively and defined as  $W^{\mu\nu} = \partial^\mu \omega^\nu - \partial^\nu \omega^\mu$  and  $\vec{R}^{\mu\nu} = \partial^\mu \vec{\rho}^\nu - \partial^\nu \vec{\rho}^\mu$ . The  $\vec{\tau}$  are the Pauli matrices and behave as the isospin operator. The saturation properties of the NM are given in Table 1 for 30 parameter sets.

We calculate the different meson fields using the Euler-Lagrangian equation of motion. We solve all the equation of motion in a self-consistent way. From the energy-momentum tensor, we

calculate the energy density ( $\mathcal{E}_{nucl.}$ ) and pressure ( $P_{nucl.}$ ).

$$\begin{aligned} \mathcal{E}_{nucl.} = & \frac{\gamma}{(2\pi)^3} \sum_{i=p,n} \int_0^{k_i} d^3k E_i^*(k_i) + \rho_b W + \frac{1}{2} \rho_3 R \\ & + \frac{m_s^2 \Phi^2}{g_s^2} \left( \frac{1}{2} + \frac{\kappa_3}{3!} \frac{\Phi}{M_{nucl.}} + \frac{\kappa_4}{4!} \frac{\Phi^2}{M_{nucl.}^2} \right) - \frac{1}{4!} \frac{\zeta_0 W^4}{g_\omega^2} \\ & - \frac{1}{2} m_\omega^2 \frac{W^2}{g_\omega^2} \left( 1 + \eta_1 \frac{\Phi}{M_{nucl.}} + \frac{\eta_2}{2} \frac{\Phi^2}{M_{nucl.}^2} \right) \\ & - \Lambda_\omega (R^2 \times W^2) - \frac{1}{2} \left( 1 + \frac{\eta_\rho \Phi}{M_{nucl.}} \right) \frac{m_\rho^2}{g_\rho^2} R^2 \\ & + \frac{1}{2} \frac{m_\delta^2}{g_\delta^2} D^2, \end{aligned} \quad (2)$$

$$\begin{aligned} P_{nucl.} = & \frac{\gamma}{3(2\pi)^3} \sum_{i=p,n} \int_0^{k_i} d^3k \frac{k^2}{E_i^*(k_i)} + \frac{1}{4!} \frac{\zeta_0 W^4}{g_\omega^2} \\ & - \frac{m_s^2 \Phi^2}{g_s^2} \left( \frac{1}{2} + \frac{\kappa_3}{3!} \frac{\Phi}{M_{nucl.}} + \frac{\kappa_4}{4!} \frac{\Phi^2}{M_{nucl.}^2} \right) \\ & + \frac{1}{2} m_\omega^2 \frac{W^2}{g_\omega^2} \left( 1 + \eta_1 \frac{\Phi}{M_{nucl.}} + \frac{\eta_2}{2} \frac{\Phi^2}{M_{nucl.}^2} \right) \\ & + \Lambda_\omega (R^2 \times W^2) + \frac{1}{2} \left( 1 + \frac{\eta_\rho \Phi}{M_{nucl.}} \right) \frac{m_\rho^2}{g_\rho^2} R^2 \\ & - \frac{1}{2} \frac{m_\delta^2}{g_\delta^2} D^2. \end{aligned} \quad (3)$$

Where  $\Phi$ ,  $W$ ,  $R$  and  $D$  are the redefined fields for  $\sigma$ ,  $\omega$ ,  $\rho$  and  $\delta$  mesons as  $\Phi = g_s \sigma^0$ ,  $W = g_\omega \omega^0$ ,  $R = g_\rho \vec{\rho}^0$  and  $D = g_\delta \delta^0$  respectively. The  $E_i^*(k_i) = \sqrt{k_i^2 + M_i^{*2}}$ , where  $M_i^*$  is the effective mass and  $k_i$  is the momentum of the nucleon and  $\gamma$  is the isospin degeneracy factor which is equal to 2 for individual nucleons.

Inside the NS, many particles like hyperons, nucleons and leptons are present. The neutron decays to proton, electron and anti-neutrino inside the NS (Glendenning 1997). This process is called as  $\beta$ -decay. To maintain the charge neutrality condition, the inverse  $\beta$ -decay process occurred. The process can be expressed as (Glendenning 1997)



To maintain the stability of NSs, there must have both  $\beta$ -equilibrium and charge-neutrality conditions is

$$\begin{aligned} \mu_n & = \mu_p + \mu_e, \\ \mu_e & = \mu_\mu, \\ \rho_p & = \rho_e + \rho_\mu. \end{aligned} \quad (5)$$

where,  $\mu_n$ ,  $\mu_p$ ,  $\mu_e$ , and  $\mu_\mu$  are the chemical potentials of neutrons, protons, electrons, and muons, respectively. When the chemical potential of electrons is equal to the muons rest mass, then muons appear inside the NS. The chemical potentials  $\mu_n$ ,  $\mu_p$ ,  $\mu_e$ , and  $\mu_\mu$  are given by (Das et al. 2020c)

$$\mu_{n,p} = g_\omega \omega_0 \pm g_\rho \rho_0 \mp g_\delta \delta_0 + \sqrt{k_{n,p}^2 + (M_{n,p}^*)^2}, \quad (6)$$

**Table 1.** The NM properties like saturation density  $\rho_0$ , incompressibility  $K$ , binding energy per particle  $-E/A$ , symmetry energy  $J$  and effective mass ratio  $M^*/M$  are given at saturation density for 30 RMF parameter sets.

Parameter Sets	$\rho_0$ (fm <sup>-3</sup> )	$K$ (MeV)	$-E/A$ (MeV)	$J$ (MeV)	$M^*/M$
HS	0.148	545.0	15.75	35.00	0.541
LA	0.148	546.8	15.75	35.00	0.540
L1	0.152	626.3	18.59	21.70	0.530
L3	0.154	212.0	16.43	43.60	0.571
NL3	0.148	271.5	16.24	37.28	0.595
NL3*	0.150	258.2	16.31	38.68	0.594
NL1	0.153	211.4	16.48	43.70	0.570
NL-SH	0.146	354.9	16.32	36.10	0.600
GM1	0.153	300.0	16.30	32.50	0.700
GL85	0.145	285.0	15.95	36.80	0.770
GL97	0.153	240.0	16.30	32.50	0.780
NL3-II	0.149	272.1	16.29	37.70	0.600
NLD	0.148	342.9	15.75	35.00	0.700
NL-RA1	0.146	285.0	16.15	36.10	0.600
TM1	0.145	281.0	16.30	36.90	0.634
TM2	0.132	344.0	16.20	35.80	0.571
PK1	0.148	282.6	16.27	37.60	0.605
FSU	0.148	230.0	16.30	32.59	0.610
FSU2	0.150	238.0	16.28	37.62	0.593
IFSU	0.155	231.2	16.40	31.30	0.589
IFSU*	0.150	236.0	16.10	29.85	0.589
SINPA	0.151	203.0	16.00	31.20	0.580
SINPB	0.150	206.0	16.04	33.95	0.590
G1	0.153	215.0	16.14	38.50	0.634
G2	0.154	215.0	16.07	36.40	0.664
G3	0.148	243.9	16.02	31.84	0.699
IOPB-I	0.149	222.6	16.10	33.30	0.593
FSUGarnet	0.153	229.5	16.23	31.84	0.578
FSU2R	0.150	238.0	16.28	30.2	0.593
FSU2H	0.150	238.0	16.28	30.2	0.593

$$\mu_{e,\mu} = \sqrt{k_{e,\mu}^2 + m_{e,\mu}^2}, \quad (7)$$

where  $M_n^*$  and  $M_p^*$  are the effective mass of neutron and proton respectively. The particle fraction inside the NS is calculated by solving Eq. (5) using the Eqs. (6–7) for a given baryon density by self-consistently. The energy density and pressure of NS are given by,

$$\begin{aligned} \mathcal{E}_{NS} &= \mathcal{E}_{nucl.} + \mathcal{E}_l, \\ \text{and } P_{NS} &= P_{nucl.} + P_l, \end{aligned} \quad (8)$$

where,

$$\mathcal{E}_l = \sum_{l=e,\mu} \frac{2}{(2\pi)^3} \int_0^{k_l} d^3k \sqrt{k^2 + m_l^2}, \quad (9)$$

and

$$P_l = \sum_{l=e,\mu} \frac{2}{3(2\pi)^3} \int_0^{k_l} \frac{d^3k k^2}{\sqrt{k^2 + m_l^2}}. \quad (10)$$

Where  $\mathcal{E}_l$ ,  $P_l$  and  $k_l$  are the energy density, pressure and Fermi momentum for leptons respectively. The Eq. (8) gives the total energy, pressure of the NS.

## 2.2 Mass and Radius of the NS

Here we want to calculate the NS observables like  $M$  and  $R$  etc. using TOV equations. Hence, we take the EOS of NS as input to the TOV equations (Tolman 1939; Oppenheimer & Volkoff 1939) are given as follow

$$\frac{dP_{tot.}(r)}{dr} = -\frac{(P_{tot.}(r) + \mathcal{E}_{tot.}(r))(m(r) + 4\pi r^3 P_{tot.}(r))}{r(r - 2m(r))}, \quad (11)$$

and

$$\frac{dm(r)}{dr} = 4\pi r^2 \mathcal{E}_{tot.}(r), \quad (12)$$

where  $\mathcal{E}_{tot.}(r)$  and  $P_{tot.}(r)$  are the total energy and pressure density as a function of radial distance.  $m(r)$  is the gravitational mass, and  $r$  is the radial parameter. These two coupled equations are solved with the boundary conditions  $\mathcal{E}(0) = \mathcal{E}_c$ ,  $m(0) = 0$ ,  $P_{tot.}(R) = 0$ , and  $m(R) = M$  to get the mass and radius of the NS at certain central density.

## 2.3 Mathematical form for different curvature

In this Subsection, we adopt the mathematical form of different quantities from (Ekşi et al. 2014), which measure the space-time curvature both inside and outside the compact objects. Several curvatures are Riemann tensor, Ricci tensor, Ricci scalar and Weyl tensor are calculated in Ref. (Ekşi et al. 2014) to measure the curvature of the space-time.

The Ricci scalar

$$\mathcal{R}(r) = 8\pi \left[ \mathcal{E}_{tot.}(r) - 3P_{tot.}(r) \right], \quad (13)$$

the full contraction of the Ricci tensor

$$\mathcal{J}(r) \equiv \sqrt{\mathcal{R}_{\mu\nu}\mathcal{R}^{\mu\nu}} = \left[ (8\pi)^2 \left[ \mathcal{E}_{tot.}^2(r) + 3P_{tot.}^2(r) \right] \right]^{1/2}, \quad (14)$$

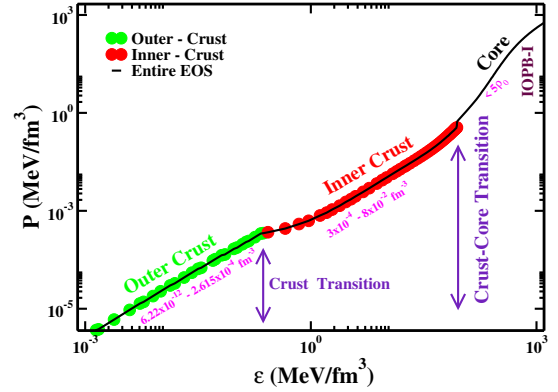


**Figure 1.** (color online) The EOS for the IOPB-I parameter set is adopted from (Das et al. 2020a). The green shaded and the red shaded region show the outer and inner crust respectively. The black solid line represents the core of the NS.

the Kretschmann scalar (full contraction of the Riemann tensor)

$$\begin{aligned} \mathcal{K}(r) &\equiv \sqrt{\mathcal{R}^{\mu\nu\rho\sigma}\mathcal{R}_{\mu\nu\rho\sigma}} \\ &= \left[ (8\pi)^2 \left[ 3\mathcal{E}_{tot.}^2(r) + 3P_{tot.}^2(r) + 2P_{tot.}(r)\mathcal{E}_{tot.}(r) \right] \right. \\ &\quad \left. - \frac{128\mathcal{E}_{tot.}(r)m(r)}{r^3} + \frac{48m^2(r)}{r^6} \right]^{1/2}, \end{aligned} \quad (15)$$

and the full contraction of the Weyl tensor

$$\mathcal{W}(r) \equiv \sqrt{C^{\mu\nu\rho\sigma}C_{\mu\nu\rho\sigma}} = \left[ \frac{4}{3} \left( \frac{6m(r)}{r^3} - 8\pi\mathcal{E}_{tot.}(r) \right)^2 \right]^{1/2}. \quad (16)$$

Where  $\mathcal{E}_{tot.}$ ,  $P_{tot.}$ ,  $m(r)$  and  $r$  are the energy density, pressure, mass and radius of the NS respectively. At the surface  $m \rightarrow M$  due to  $r \rightarrow R$ . The Ricci tensor and Ricci scalar vanish outside the star because they depend on the  $\mathcal{E}_{tot.}(r)$ ,  $P_{tot.}(r)$ , which are zero outside the star. But, there is a non-vanishing component of the Riemann tensor which does not vanish;  $\mathcal{R}^1_{010} = -\frac{2M}{R^3} = -\xi$ , even in the outside of the star (Ekşi et al. 2014; He et al. 2015). So the Riemann tensor is the more relevant quantity to measure the curvature of the stars than others. Kretschmann scalar is the square root of the full contraction of the Riemann tensor. The vacuum value for both  $\mathcal{K}$  and  $\mathcal{W}$  is  $\frac{4\sqrt{3}M}{R^3}$ , one can easily see from Eqs. (15) and (16). Therefore, one can take  $\mathcal{K}$  and  $\mathcal{W}$  as two reasonable measures for the curvature within the star.

## 3 RESULTS AND DISCUSSIONS

The structure of an NS is divided into the four regions outer crust, inner crust, outer core and inner core. The outer crust consists of nuclei distributed in a solid body-centred-cubic (bcc) lattice filled by a free electron gas. As we go from outer crust to inner crust, the density increases and eventually the nuclei in the crust become so neutron-rich that neutrons start to drip from them. In this situation, the inner crust contains the free electron and neutron gases and formed different types of pasta structure. With the help of nuclear models, the neutron drip density determined the boundary between the outer and inner crust. But, the transition density from the crust to the core is much more uncertain and strongly model-dependent.

When the average density reaches a value about half of the NM saturation density, the lattice structure escapes due to energetic reasons and the system changes to a liquid phase. In Fig. 1, we show IOPB-I as the representative EOS of the RMF model. The lowest density part of the EOS represents the outer crust of the NS. The inner crust ranges from a density  $3 \times 10^{-4}$  to  $8 \times 10^{-2} \text{ fm}^{-3}$ . The core part starts from a density  $2 \times 10^{-2} \text{ fm}^{-3}$  and it extends up to the centre of the NS, which is 5–6 times the density of the NM ( $0.16 \text{ fm}^{-3}$ ). The EOS for all other parameter sets have similar qualitative nature, only they differ quantitatively. The EOS for the outer and inner crust are the same for all the parameter sets, we use the BCPM EOS by Sharma *et al.* (Sharma *et al.* 2015) for these parts of the NS. In the present context, we take 30 well-known parameter sets of the RMF model to study various properties of the NS and investigate the existing co-relation between various quantities. These parameter sets are HS (Horowitz & Serot 1981), LA (Furnstahl *et al.* 1987), H1 (Haddad 1999), LZ (Reinhard 1989), NL3 (Lalazissis *et al.* 1997), NL3\* (Lalazissis *et al.* 2009), NL-SH (Sharma *et al.* 1993), NL1 (Reinhard *et al.* 1986), GM1 (Glendenning & Moszkowski 1991), GL85 (Glendenning 1985), GL97 (Glendenning 1997), NL3-II (Lalazissis *et al.* 1997), NLD (Furnstahl *et al.* 1987), NL-RA1 (Rashdan 2001), TM1 (Sugahara & Toki 1994), TM2 (Sugahara & Toki 1994), PK1 (Long *et al.* 2004), FSU (Todd-Rutel & Piekarewicz 2005), FSU2 (Chen & Piekarewicz 2014), IUFSU (Fattoyev *et al.* 2010), IUFSU\* (Fattoyev & Piekarewicz 2010), SINPA (Mondal *et al.* 2016), SINPB (Mondal *et al.* 2016), G1 (Furnstahl *et al.* 1997), G2 (Furnstahl *et al.* 1997), G3 (Kumar *et al.* 2017a), IOPB-I (Kumar *et al.* 2018), FSUGarnet (Chen & Piekarewicz 2015), FSU2R (Tolos *et al.* 2016), and FSU2H (Tolos *et al.* 2016). All parameter sets cover a wide range of the NM properties. The incompressibility ( $K$ ) values range from 211 MeV for LZ parameter set to 584 MeV for the NL1 parameter sets. Similarly, the symmetry energy also covers a wide range 25.93 MeV for H1 to 43.7 MeV for NL1 parameter set. The main idea to take a large sets of the parameter sets is to cover the wide range of the NM parameter value and second to establish a correlation with more accuracy.

In Fig. 2, we show the mass-radius relation for 30 assumed RMF parameter sets. We also put the masses of pulsar like PSR J1614-2230 (Demorest *et al.* 2010), PSR J0348+0432 (Antoniadis *et al.* 2013) and PSR J0740+6620 (Cromartie *et al.* 2019). The mass-radius of the two companion stars from the GW170817 event are shown in shaded regions. Recently, the secondary components of the GW190814 events left us to speculate whether it is the lowest massive black hole (BH) or a super heavy NS. The observed mass was  $2.50\text{--}2.67 M_{\odot}$ . Many authors have claimed that it was a binary BH merger (Fattoyev *et al.* 2020; Das *et al.* 2020b), heaviest NS (Tan *et al.* 2020; Huang *et al.* 2020), super-fast pulsar (Zhang & Li 2020) etc. The NICER results also put a constraint on both mass-radius from the x-ray study of the millisecond pulsars PSR J0030+0451 (Miller *et al.* 2019). The constraint on mass-radius is found to be  $M = 1.44^{+0.15}_{-0.14} M_{\odot}$ ,  $R = 13.02^{+1.24}_{-1.06}$  km and which is indicated in green double bar line.

Few parameter sets lie in the range of the observed maximum masses. These parameter sets are GL97, GL85, PK1, FSU2, IUFSU\*, SINPA, SINPB, G1, G2, G3, and IOPB-I. Most of the RMF parameter sets satisfy the mass-radius constraint from the NICER observation. We can see from the Fig. 2, the NICER data can not discard many EOS based on the mass-radius measurement. The NICER data is related to the radius measurement of the NS of mass around  $1.4 M_{\odot}$ , which has not very high central density. The central density of the canonical NS lies  $2\text{--}3 \rho_0$ . As all the EOS are fitted to the saturation properties, they show a convergent behaviour up to a

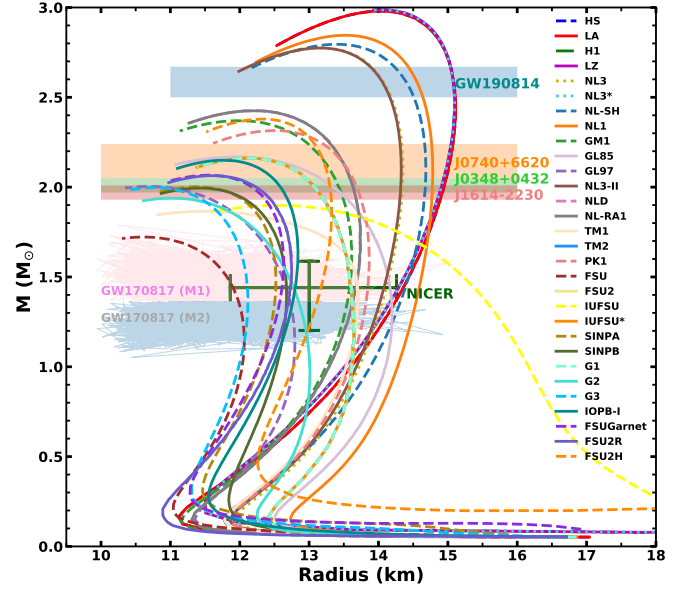


**Figure 2.** (colour online) Mass and radius of the NS for 30 parameter sets are depicted. The recent observational constraints from GW190814 along with different pulsars J0740+6620, J0348+0432 and J1614-2230 are shown with horizontal bars. The mass and radius of the two companion stars in the merger of binary NS event GW170817 are shown by the shaded area. The mass-radius relation observed by the NICER from the study of pulsar PSR J0030+0451 is also shown.

few times the saturation density. This also a fact that the properties of the small NS have a strong correlation with the properties of the NM, due to their low central density (Carriere *et al.* 2003). Few parameter sets like NL3, NL1, HS, LA, and FSU parameter sets do not obey the NICER mass-radius constraint. But only 7 parameter sets like SINPB, GL97, FSU2R, FSUGarnet, IOPB-I, G1, and GL85 obey both the NICER and maximum NS mass constraints. If we, put tidal deformability constraint of the GW170817 (Abbott *et al.* 2018, 2017), then only a few parameter sets like GL97, SINPB, IOPB-I and FSUGarnet can satisfy all the constraints.

### 3.1 Radius of the canonical NS

Along with the maximum mass, in recent years the radius of the canonical star is also used as an important constraint to control the nature of the EOS in the high density region (Fattoyev *et al.* 2010). It is now a well-known fact that the radius of the canonical NS and the canonical tidal deformability are strongly correlated (Nandi *et al.* 2019; Lourenço *et al.* 2020; Malik *et al.* 2018). Various models give a different form of correlation. Different analysis of tidal deformability data of GW170817 suggest different range of canonical radius (Malik *et al.* 2018; Hebeler *et al.* 2010; Lim & Holt 2018; Most *et al.* 2018; Fattoyev *et al.* 2018; Lourenço *et al.* 2020; Tews *et al.* 2018; Annala *et al.* 2018; Zhang *et al.* 2018; Dietrich *et al.* 2020; Capano *et al.* 2019; De *et al.* 2018; Köppel *et al.* 2019; Montaña *et al.* 2019; Radice & Dai 2019; Coughlin *et al.* 2019; Kumar & Landry 2019). We plot the ranges of the canonical radius in the Fig. 3. In some cases, the analysis shows a very narrow range of the canonical radius for example in references Most *et al.* 2018 (Most *et al.* 2018). But in many cases, the acceptable range is too wide, which is not much suitable to constraint the EOS. If we consider the maximum and minimum radius predicted by the

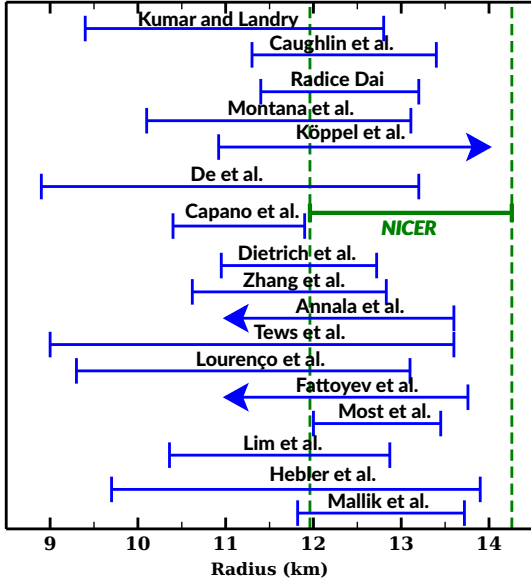


**Figure 3.** (color online) We compile the ranges of the canonical radius from some refs. (Malik et al. 2018; Hebeler et al. 2010; Lim & Holt 2018; Most et al. 2018; Fattoyev et al. 2018; Lourenço et al. 2020; Tews et al. 2018; Annala et al. 2018; Zhang et al. 2018; Dietrich et al. 2020; Capano et al. 2019; De et al. 2018; Köppel et al. 2019; Montaña et al. 2019; Radice & Dai 2019; Coughlin et al. 2019; Kumar & Landry 2019). The left and right arrow represents no fixed lower and upper limit for canonical NS as compare to others. The NICER radius range given by Miller *et al.* (Miller et al. 2019) also depicted with solid green line.

RMF parameter sets, we can find the radius range of the canonical star in the range 11.4–13.9 km, which completely lies in the range reported in the NICER experiment (Miller et al. 2019). This shows that RMF formalism is good enough to reproduce the NICER data. If we do not consider the maximum mass limit and stick to the NICER constraint only, then almost all RMF parameter obey the mass-radius constraint. From Fig. 2, it is clear that too soft EOS (low maximum mass) and too stiff EOS (high maximum mass) are discarded by both NICER and maximum mass constraint.

In Fig. 3, we compile the canonical radius of the NS predicted from different approaches. We present the NICER results on top of it with solid green line. The upper limit of the canonical radius from various approaches lies in the range of NICER result. But the lower limit of most of the approaches lies outside the NICER result. The range of the canonical star given by Most *et al.* lies completely within the range of NICER result. More than 50% limit is satisfied by Mallik *et al.*, Fattoyev *et al.*, Annala *et al.*, Radice *et al.* and Coughlin *et al.*.

### 3.2 Correlation between compactness and curvature

The compactness of the NS is defined as the ratio of the mass and the corresponding radius. In Fig. 4, we plot the compactness with the curvature with various parameter sets of the RMF model for the canonical star. The graph shows that there is a strong correlation between the compactness and curvature of the canonical star. The correlation looks linear and the value of the correlation coefficient shows that these quantities are strongly correlated. The correlation coefficient is 0.95 for the canonical star. One can see the data from various parameter sets and the fitted line are almost overlap.

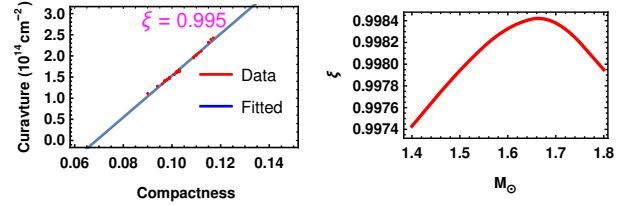


**Figure 4.** (color online) Left: We plot the surface curvature with compactness for canonical star for various parameter sets of the RMF model. We find a positive correlation (with co-efficient  $\zeta = 0.995$ ) between them. Right: The calculated correlation coefficient using Pearson formula for the surface curvature and compactness with different masses of the NS is shown.

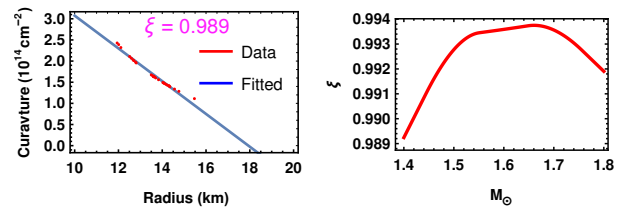


**Figure 5.** (color online) Left: We plot the surface curvatures with radius for canonical star for various parameter sets of the RMF model. We find a negative correlation (with co-efficient  $\zeta = 0.989$ ) between them. Right: The calculated correlation coefficient using Pearson formula for the surface curvature and radius with different masses of the NS is shown.

This correlation is monotonically increasing. A parameter set having higher curvature shows higher compactness also. We have also studied a three-dimensional correlation between the curvature and compactness at different mass of the NS. We use a formula, which is already used in (Zimmerman et al. 2020) to calculate the three-dimensional correlation between various properties of NM and NS. We define the correlation co-efficient

$$\xi = \frac{\sum_{xy}}{\sqrt{\sum_{xx}\sum_{yy}}}, \quad (17)$$

where

$$\sum_{xy} = \frac{1}{N} \sum_{i=0}^N x_i y_i - \frac{1}{N^2} \left( \sum_{i=0}^N x_i \right) \left( \sum_{i=0}^N y_i \right). \quad (18)$$

These equations are used to calculate the correlation. In the right panel of Fig. 4, we plot the correlation coefficient with a different mass. We can see from the graph that the value of the  $\xi$  is maximum at a particular value of the mass and it decreases below and above this value. We can say the curvature and the compactness are highly correlated around this mass of the NS or corresponding that central density. The value of the coefficient is maximum around  $1.7 M_{\odot}$ . We plot, the curvature and radius of the different parameter set of the RMF model in Fig. 5. We find a correlation between the curvature and radius of the NS of the RMF model. We fit a linear curve to the data point, and it is found matching well. The correlation coefficient found to be 0.98. This correlation is comparatively weaker than the correlation between the compactness and curvature. For the three-dimensional correlation between the curvature, radius and mass, we plot in Fig. 5 the correlation coefficient calculated using Eqs. (17) and (18) with mass. Unlike the former case, here you do not find any pick at a particular mass of the NS. We find a flat curve

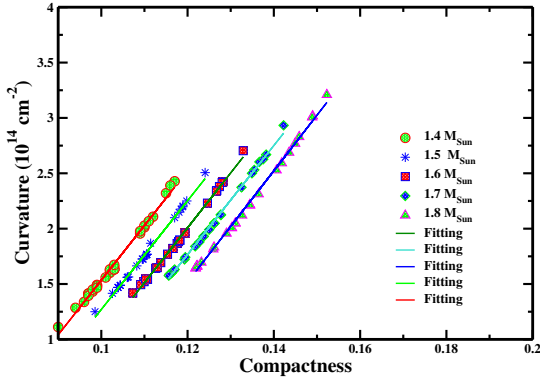


**Figure 6.** (color online) The correlation between surface curvature and compactness for considered parameter sets is shown for different masses of the NS.

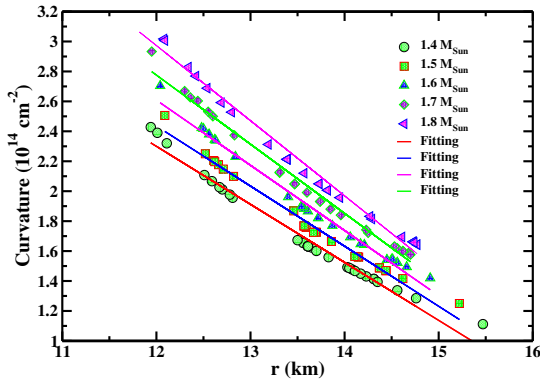


**Figure 7.** (color online) The correlation between surface curvature and radius at the different masses of the NS for considered parameter sets is shown.

in the range of mass  $1.5 M_{\odot}$  and  $1.7 M_{\odot}$ . Though the curve has not a very sharp peak at  $1.7 M_{\odot}$ , still it shows a local maximum of around  $1.7 M_{\odot}$ . To show more specifically the mass dependence, we plot the Fig. 7 and 8. We plot the curvature and radius of the NS for the different parameter sets of the RMF model for the different mass of the NS in Fig. 7. We can see from the graph that there a correlation at each mass of the NS. We calculated the correlation between a pair of quantities using Eqs. (17) and (18) and present in Fig. 8. The  $8 \times 8$  matrix which represents the correlations between a pair of quantities and the correlations coefficients are written inside the box. We find a noticeable correlation between curvature with radius and compactness. There is a strong correlation between these pairs  $\mathcal{K}_{1.4}-R_{1.4}$ ,  $\mathcal{K}_{1.4}-C_{1.4}$ . Therefore, we conclude that a very strong correlation between curvature, radius and compactness of the NS. Finally, we tabulated all the calculated quantities of the NS in Table 2. We listed the pressure at supra-saturation density, central density, maximum mass, radius, surface curvature and the compactness of the NS. We can see from the table that the parameter sets which has high maximum mass, the pressure at supra-saturation density for the corresponding parameter sets exceed the range given by the GW170817 data (Abbott et al. 2018). For example, the NL3 parameter set has a maximum mass  $2.774 M_{\odot}$  and the corresponding pressure at  $2\rho_0$  is 40.48 MeV. From the table, it is clear that the linear parameter sets like LA and others have very high pressure at  $2\rho_0$ .

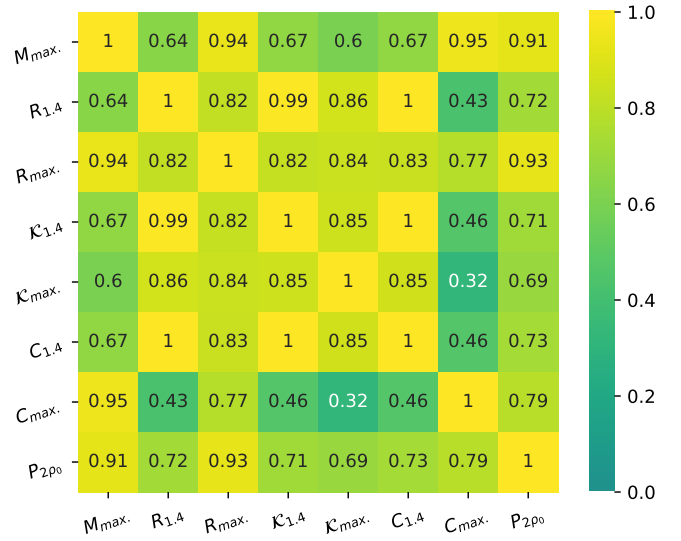


**Figure 8.** (color online) The heat map plot represents the correlation between different quantities like  $M_{max.}$ ,  $R_{1.4}$ ,  $R_{max.}$ ,  $\mathcal{K}_{1.4}$ ,  $\mathcal{K}_{max.}$ ,  $C_{1.4}$ ,  $C_{max.}$  and  $P_{2\rho_0}$ . Each number inside the box represents the correlation co-efficients calculated using the Pearson formula between that corresponding pair.

## 4 CONCLUSIONS

In summary, we study the correlations of various quantities such as mass, radius, curvatures and compactness of NS obtained from various relativistic mean parameter sets. Since the last four decades, the RMF formalism has been well suited for the study of NM and NS properties. To study the correlations, we have taken 30 different RMF EOS, which cover a wider range of nuclear saturation properties. We have analysed the range of the canonical radius from different approaches. We have also compared the RMF results with NICER data. We found that the lower limit of the canonical radius from different approaches lies outside the NICER data except for Most *et al.* data. But still, the upper limit of the canonical radius of different approaches lie within the range of the NICER data. Also, we have seen that only a few parameter sets can satisfy both the maximum mass and NICER constraints. From the Fig. 2, it is clear that the none of the parameter sets can satisfy both the constraint from GW170817 and GW190814. There are only a few parameters sets NL3, NL3II, NL3\*, NLRA1 and H1, which satisfy the constraint from NICER, GW190814 and the observed maximum mass of NS. We can choose the most suitable parameter sets, which obey simultaneously the constraints from NICER, GW170817 and maximum mass limit. These parameters are FSUGarnet, FSU2R, FSU2H, FSU, IOPB-I, TM2, G1. This analysis shows that some parameter sets can reproduce the maximum mass of the supermassive neutron star ( not confirmed yet supermassive NS or smallest black hole ) but simultaneously unable to reproduce other constraints. So it gives a hint that we can modify these equations of state in the lower density region to satisfy the constraints from the GW170817 and NICER data. We have calculated the curvature of the neutron star using RMF model. The interesting conclusion is we found a correlation exists between curvature and compactness at different masses of the neutron star. They follow a linear correlation between them. Using Pearson formula, we have calculated the correlation coefficient. We found the correlation coefficient between the curvature and compactness is  $\zeta = 0.995$ . The co-efficient value shows that the correlation is strong enough. Similarly, we found another correlation between the curvature and the radius of the neutron star, having the correlation coefficient  $\zeta = 0.989$ .

**Table 2.** We tabulate the various properties of NS namely pressure at two times saturation density, maximum mass ( $M$ ), radius ( $R$ ), central density ( $\mathcal{E}_c$ ), curvature at the surface ( $\mathcal{K}(R)$ ) and compactness ( $C$ ).

Parameter sets	Pressure ( $2\rho_0$ )	$M$ ( $M_\odot$ )	$R$ (km)		$\mathcal{E}_c$ ( $\text{MeV fm}^{-3}$ )		$\mathcal{K}(R)$ ( $10^{14}\mathcal{K}_\odot$ )		$C$ ( $M_\odot\text{km}^{-1}$ )	
			$R_{1.4}$	$R_{max.}$	$\mathcal{E}_{1.4}$	$\mathcal{E}_{max.}$	$\mathcal{K}_{1.4}$	$\mathcal{K}_{max.}$	$C_{1.4}$	$C_{max.}$
HS	58.22	2.980	14.31	14.03	226	750	1.414	3.183	0.097	0.212
LA	58.22	2.980	14.31	14.03	226	750	1.414	3.183	0.097	0.212
H1	57.71	2.987	14.23	14.03	226	750	1.431	3.188	0.098	0.213
LZ	60.47	2.981	14.76	14.16	226	740	1.285	3.095	0.094	0.210
NL3	40.48	2.774	14.08	13.16	270	870	1.477	3.584	0.099	0.210
NL3*	41.41	2.760	14.03	13.11	276	870	1.492	3.610	0.099	0.211
NL1	51.50	2.845	14.56	13.51	254	830	1.338	3.397	0.096	0.210
NL-SH	43.70	2.795	14.35	13.42	249	830	1.394	3.141	0.097	0.210
GM1	33.00	2.370	13.56	11.96	314	1100	1.654	4.085	0.103	0.208
GL85	28.00	2.168	14.17	11.93	311	1150	1.449	3.769	0.098	0.198
GL97	23.10	2.003	12.70	10.67	440	1440	2.012	4.865	0.110	0.181
NL3-II	41.22	2.774	14.05	13.15	271	870	1.487	3.593	0.099	0.188
NLD	32.08	2.425	13.65	12.28	302	1000	1.624	3.857	0.102	0.210
NL-RA1	39.60	2.785	14.11	13.23	265	860	1.467	3.548	0.099	0.197
TM1	27.30	1.865	13.70	11.50	332	1240	1.601	3.616	0.102	0.210
TM2	21.30	2.161	13.61	12.07	344	1100	1.632	3.619	0.103	0.162
PK1	31.61	2.314	13.83	12.48	304	1000	1.559	3.507	0.101	0.179
FSU	18.20	1.722	11.94	10.62	540	1390	2.428	4.247	0.117	0.185
FSU2	27.20	2.161	13.61	12.07	344	1100	1.632	3.619	0.102	0.162
IFSU	31.61	1.898	15.47	12.54	310	1100	1.112	2.837	0.090	0.151
IFSU*	22.20	2.161	13.61	12.07	344	1100	1.632	3.619	0.103	0.179
SINPA	25.90	2.002	12.51	11.37	405	1190	2.108	4.012	0.112	0.176
SINPB	23.70	1.994	12.67	11.44	402	1180	2.027	3.930	0.110	0.174
G1	31.86	2.161	13.61	12.07	344	1100	1.632	3.619	0.103	0.179
G2	25.22	1.938	12.81	11.02	443	1342	1.956	4.286	0.109	0.176
G3	19.14	1.997	12.11	10.80	460	1325	2.320	4.726	0.115	0.185
IOPB-I	25.07	2.149	12.78	11.76	366	1100	1.977	3.893	0.109	0.182
FSUGarnet	26.51	2.066	12.59	11.57	384	1130	2.067	3.934	0.111	0.178
FSU2R	18.86	2.063	12.72	11.61	375	1130	2.004	3.888	0.110	0.177
FSU2H	26.44	2.379	13.14	12.32	327	1000	1.819	3.752	0.106	0.181

**REFERENCES**

- Abbott B. P., et al., 2017, *Phys. Rev. Lett.*, 119, 161101  
Abbott B. P., et al., 2018, *Phys. Rev. Lett.*, 121, 161101  
Alam N., Agrawal B. K., Fortin M., Pais H., Providência C., Raduta A. R., Sulaksono A., 2016, *Phys. Rev. C*, 94, 052801  
Ambartsumyan V. A., Saakyan G. S., 1960, *Sov. Astron.*, 4  
Annala E., Gorda T., Kurkela A., Vuorinen A., 2018, *Phys. Rev. Lett.*, 120, 172703  
Antoniadis J., et al., 2013, *Science*, 340  
Baym G., Pethick C., 1979, *Annual Review of Astronomy and Astrophysics*, 17, 415  
Bhat S. A., Paul A., 2020, *The European Physical Journal C*, 80, 544  
Bilous A. V., Watts A. L., Harding A. K., et al., 2019, *The Astrophysical Journal*, 887, L23  
Bogdanov S., Lamb F. K., Mahmoodifar S., et al., 2019, *The Astrophysical Journal*, 887, L26  
Boguta J., Bodmer A., 1977, *Nucl. Phys. A*, 292, 413

- Brockmann R., Weise W., 1977, *Phys. Rev. C*, 16, 1282
- Capano C. D., Tews I., et al., 2019 ([arXiv:1908.10352](#))
- Carriere J., Horowitz C. J., Piekarewicz J., 2003, *The Astrophysical Journal*, 593, 463
- Chen W.-C., Piekarewicz J., 2014, *Phys. Rev. C*, 90, 044305
- Chen W.-C., Piekarewicz J., 2015, *Physics Letters B*, 748, 284
- Chin S. A., Walecka J. D., 1974, *Phys. Lett. B*, 52, 24
- Christiansen M. B., Glendenning N. K., Schaffner-Bielich J., 2000, *Phys. Rev. C*, 62, 025804
- Ciarcelluti P., Sandin F., 2011, *Phys. Lett. B*, 695, 19–21
- Collins J. C., Perry M. J., 1975, *Physical Review Letters*, 34, 1353
- Coughlin M. W., Dietrich T., Margalit B., Metzger B. D., 2019, *Monthly Notices of the Royal Astronomical Society: Letters*, 489, L91–L96
- Cromartie T. H., Fonseca E., Ransom S. M., et al., 2019, *arXiv e-prints*, p. [arXiv:1904.06759](#)
- Danielewicz P., Lee J., 2014, *Nucl. Phys. A*, 922, 1
- Das A., Malik T., Nayak A. C., 2019, *Phys. Rev. D*, 99
- Das H. C., Kumar A., Kumar B., Biswal S. K., Patra S. K., 2020a ([arXiv:2007.05382](#))
- Das H. C., Kumar A., Kumar B., Biswal S. K., Patra S. K., 2020b ([arXiv:2009.10690](#))
- Das H. C., Kumar A., Kumar B., et al., 2020c, *MNRAS*, 495, 4893
- De S., Finstad D., Lattimer J. M., Brown D. A., Berger E., Biwer C. M., 2018, *Phys. Rev. Lett.*, 121, 091102
- Demorest P. B., et al., 2010, *Nature*, 467, 1081
- Dexheimer V., Soethe L. T. T., Roark J., et al., 2018, *International Journal of Modern Physics E*, 27, 1830008
- Dietrich T., Coughlin M. W., Pang P. T. H., et al., 2020 ([arXiv:2002.11355](#))
- Dutra M., Lourenço O., Avancini S. S., et al., 2014, *Phys. Rev. C*, 90, 055203
- Ekşi K. Y., Güngör C., Türkoğlu M. M., 2014, *Phys. Rev. D*, 89, 063003
- Ellis J., Hütsi G., Kannike K., et al., 2018, *Phys. Rev. D*, 97
- Fattoyev F. J., Piekarewicz J., 2010, *Phys. Rev. C*, 82, 025805
- Fattoyev F. J., Piekarewicz J., 2012, *Phys. Rev. C*, 86, 015802
- Fattoyev F. J., Horowitz C. J., Piekarewicz J., Shen G., 2010, *Phys. Rev. C*, 82, 055803
- Fattoyev F. J., Piekarewicz J., Horowitz C. J., 2018, *Phys. Rev. Lett.*, 120, 172702
- Fattoyev F. J., Horowitz C. J., Piekarewicz J., Reed B., 2020 ([arXiv:2007.03799](#))
- Furnstahl R. J., Price C. E., Walker G. E., 1987, *Phys. Rev. C*, 36, 2590
- Furnstahl R. J., Serot B. D., Tang H.-B., 1997, *Nucl. Phys. A*, 615, 441
- Gambhir Y., Ring P., Thimet A., 1990, *Ann. Phys.*, 198, 132
- Glendenning N. K., 1985, *Astrophys. J.*, 293, 470
- Glendenning N. K., 1997, *Compact Stars : Nuclear Physics, particle Physics , and General Relativity*. Springer - Verlag, New York
- Glendenning N. K., Moszkowski S. A., 1991, *Phys. Rev. Lett.*, 67, 2414
- Glendenning N. K., Schaffner-Bielich J., 1998, *Phys. Rev. Lett.*, 81, 4564
- Glendenning N. K., Schaffner-Bielich J., 1999, *Phys. Rev. C*, 60, 025803
- Guillot S., Kerr M., Ray P. S., et al., 2019, *The Astrophysical Journal*, 887, L27
- Gupta N., Arumugam P., 2012, *Phys. Rev. C*, 85, 015804
- Gupta N., Arumugam P., 2013, *Phys. Rev. C*, 87, 028801
- Haddad S., 1999, *Europhysics Letters (EPL)*, 48, 505
- He X.-T., Fattoyev F. J., Li B.-A., Newton W. G., 2015, *Phys. Rev. C*, 91, 015810
- Hebeler K., Lattimer J. M., Pethick C. J., Schwenk A., 2010, *Phys. Rev. Lett.*, 105, 161102
- Horowitz C. J., Piekarewicz J., 2001, *Phys. Rev. C*, 64, 062802
- Horowitz C. J., Serot B. D., 1981, *Nucl. Phys. A*, 368, 503
- Huang K., Hu J., Zhang Y., Shen H., 2020 ([arXiv:2008.04491](#))
- Kumar B., Landry P., 2019, *Phys. Rev. D*, 99, 123026
- Kumar B., Biswal S. K., Patra S. K., 2017a, *Phys. Rev. C*, 95, 015801
- Kumar B., Singh S., Agrawal B., Patra S., 2017b, *Nuclear Physics A*, 966, 197
- Kumar B., Patra S. K., Agrawal B. K., 2018, *Phys. Rev. C*, 97, 045806
- Köppel S., Bovard L., Rezzolla L., 2019, *The Astrophysical Journal*, 872, L16
- Lalazissis G. A., König J., Ring P., 1997, *Phys. Rev. C*, 55, 540
- Lalazissis G. A., Karatzikos S., Fossion R., et al., 2009, *Physics Letters B*, 671, 36
- Lattimer J. M., 2004, *Science*, 304, 536
- Leung S.-C., Chu M.-C., Lin L.-M., 2011, *Phys. Rev. D*, 84
- Li B.-A., Magno M., 2020, *Phys. Rev. C*, 102, 045807
- Li A., Huang F., Xu R.-X., 2012, *Astroparticle Physics*, 37, 70–74
- Lim Y., Holt J. W., 2018, *Phys. Rev. Lett.*, 121, 062701
- Long W., Meng J., Giai N. V., Zhou S.-G., 2004, *Phys. Rev. C*, 69, 034319
- Lourenço O., Bhuyan M., Lenzi C., et al., 2020, *Physics Letters B*, 803, 135306
- Malik T., Alam N., Fortin M., et al., 2018, *Phys. Rev. C*, 98, 035804
- Meng J., Zhou S. G., 2015, *Journal of Physics G: Nuclear and Particle Physics*, 42, 093101
- Meng J., Toki H., Zhou S., Zhang S., Long W., Geng L., 2006, *Progress in Particle and Nuclear Physics*, 57, 470
- Millener D. J., Dover C. B., Gal A., 1988, *Phys. Rev. C*, 38, 2700
- Miller L. D., Green A. E. S., 1972, *Phys. Rev. C*, 5, 241
- Miller M. C., Lamb F. K., Dittmann A. J., et al., 2019, *The Astrophysical Journal*, 887, L24
- Mondal C., Agrawal B. K., De J. N., Samaddar S. K., 2016, *Phys. Rev. C*, 93, 044328
- Montaña G., Tolós L., Hanauske M., Rezzolla L., 2019, *Phys. Rev. D*, 99, 103009
- Most E. R., Weih L. R., Rezzolla L., Schaffner-Bielich J., 2018, *Phys. Rev. Lett.*, 120, 261103
- Müller H., Serot B. D., 1996, *Nuclear Physics A*, 606, 508
- Nandi R., Char P., Pal S., 2019, *Phys. Rev. C*, 99, 052802
- Nikšić T., Vretenar D., Ring P., 2011, *Progress in Particle and Nuclear Physics*, 66, 519
- Oppenheimer J. R., Volkoff G. M., 1939, *Phys. Rev.*, 55, 374
- Panotopoulos G., Lopes I., 2017, *Phys. Rev. D*, 96
- Raaïmakers G., Riley T. E., Watts A. L., et al., 2019, *The Astrophysical Journal*, 887, L22
- Radice D., Dai L., 2019, *The European Physical Journal A*, 55
- Rashdan M., 2001, *Phys. Rev. C*, 63, 044303
- Reinhard P. G., 1988, *Z. Phys. A Atomic Nuclei*, 329, 257
- Reinhard P. G., 1989, *Reports on Progress in Physics*, 52, 439
- Reinhard P. G., Rufa M., Maruhn J., Greiner W., Friedrich J., 1986, *Z. Phys. A Atomic Nuclei*, 323, 13
- Riley T. E., Watts A. L., Bogdanov S., et al., 2019, *The Astrophysical Journal*, 887, L21
- Ring P., 1996, *Progress in Particle and Nuclear Physics*, 37, 193
- Serot B. D., Walecka J. D., 1979, *Phys. Lett. B*, 87, 172
- Serot B. D., Walecka J. D., 1986, *Adv. Nucl. Phys.*, 16, 1
- Sharma M., Nagarajan M., Ring P., 1993, *Physics Letters B*, 312, 377
- Sharma B. K., Centelles, M. Viñas, X. Baldo, M. Burgio, G. F. 2015, *A&A*, 584, A103
- Steiner A. W., Lattimer J. M., Brown E. F., 2010, *The Astrophysical Journal*, 722, 33
- Sugahara Y., Toki H., 1994, *Nucl. Phys. A*, 579, 557
- Tan H., Noronha-Hostler J., Yunes N., 2020 ([arXiv:2006.16296](#))
- Tews I., Margueron J., Reddy S., 2018, *Phys. Rev. C*, 98, 045804
- Todd-Rutel B. G., Piekarewicz J., 2005, *Phys. Rev. Lett.*, 95, 122501
- Tolman R. C., 1939, *Phys. Rev.*, 55, 364
- Tolos L., Centelles M., Ramos A., 2016, *The Astrophysical Journal*, 834, 3
- Wei J.-B., Lu J.-J., Burgio G. F., Li Z.-H., Schulze H.-J., 2020, *The European Physical Journal A*, 56, 63
- Xia C.-J., Zhou S.-G., 2017, *Nucl. Phys. B*, 916, 669
- Xia C.-J., Peng G.-X., Zhao E.-G., Zhou S.-G., 2016a, *Science Bulletin*, 61, 172
- Xia C.-J., Peng G.-X., Zhao E.-G., Zhou S.-G., 2016b, *Phys. Rev. D*, 93, 085025
- Zhang N.-B., Li B.-A., 2020, *The Astrophysical Journal*, 902, 38
- Zhang N.-B., Li B.-A., Xu J., 2018, *The Astrophysical Journal*, 859, 90
- Zimmerman J., Carson Z., Schumacher K., Steiner A. W., Yagi K., 2020 ([arXiv:2002.03210](#))